Schottky barriers at transition-metal/$SrTiO_3$(001) interfaces

M. Mrovec,[1,2,*] J.-M. Albina,[1,2] B. Meyer,[3] and C. Elsässer[1,2]
[1]*Institute for Reliability of Components and Systems IZBS, University of Karlsruhe, Kaiserstrasse 12, 76131 Karlsruhe, Germany*
[2]*Fraunhofer Institute for Mechanics of Materials IWM, Wöhlerstrasse 11, 79108 Freiburg, Germany*
[3]*Interdisciplinary Center for Molecular Materials (ICMM) and Computer-Chemistry-Center (CCC), University of Erlangen-Nürnberg, Nägelsbachstrasse 25, 91052 Erlangen, Germany*
(Received 3 April 2009; revised manuscript received 13 May 2009; published 18 June 2009)

Schottky barrier heights were calculated for a series of interfaces between transition metals and strontium titanate with the first-principles mixed-basis pseudopotential method based on density-functional theory. The process of interface formation was analyzed in a step-by-step procedure that enables one to distinguish between structural and electronic contributions influencing the Schottky barrier height. This decomposition yields not only detailed information about the most relevant quantities that determine the band lineup at the interface but also provides means to validate fundamental assumptions of phenomenological theories, which estimate the Schottky barrier height from few characteristic material parameters.

DOI: 10.1103/PhysRevB.79.245121 PACS number(s): 71.15.−m, 73.30.+y, 73.40.Rw, 77.55.+f

I. INTRODUCTION

Electroceramic materials with perovskite structure are being increasingly integrated in many modern microelectronic devices (for reviews see, e.g., Refs. 1–4). Perovskite oxides have a broad range of technological applications due to their unique properties such as ferro-, piezo-, and pyroelectricity, high-T_C superconductivity, colossal magnetoresistance, or optical transparency. Because of their high dielectric permittivity they have been also frequently considered as alternative materials to classical dielectrics.

One of the key microelectronic devices that contain a thin dielectric layer is the dynamic random-access memory (DRAM). An integrated capacitor in every memory cell is typically made by a thin dielectric layer sandwiched between two electrodes. As the device dimensions continue to be reduced, dielectric materials which are used today are reaching their operational limits. To maintain the steady increase in memory capacity in the future, much work in recent years has focused on oxides with high dielectric constants such as strontium titanate (STO) and barium strontium titanate (BST) as replacements of the Si-oxide/Si-nitride dielectrics for future integrated capacitors. A similar situation exists for another fundamental building component of integrated circuits—the metal-oxide-semiconductor field-effect transistor (MOSFET). Silicon dioxide has been used as the primary gate dielectric in field-effect devices since their invention and it has already reached the thickness of less than 40 Å in today's high-performance processors. With the current rate of scaling, its thickness would reach only about 10 Å within the next decade. However, as the SiO_2 layer is thinned further, the gate leakage currents increase exponentially and make the MOSFET devices practically unusable for films thinner than 20 Å. High-k perovskite oxides such as BST are considered as possible gate insulators in future generations of MOSFET transistors.[5–7] Finally, a great attention is given to ferroelectric perovskites such as barium titanate, lead zirconate titanate, and strontium bismuth tantalate for use in nonvolatile memory devices, pyroelectric elements in infrared imaging systems, and actuators in microelectromechanical structures.

One of the crucial characteristics for the quality and reliability of integrated capacitors as well as field-effect devices is the leakage current. In the case of DRAM, leakage must be kept sufficiently low so that the capacitor does not completely discharge before it is refreshed. The reduction in the leakage currents concerns also MOSFET devices, particularly with regard to power dissipation, reliability, and lifetime. It has been observed experimentally that leakage is very sensitive to the deposition process, defect microstructure and chemistry, but in miniaturized systems, where interfaces play an important role, it is primarily affected by the structure and composition of film-electrode interfaces.

The basic understanding of leakage properties of thin perovskite films is based on the formation of a potential barrier at the interface between the insulating film and the metal electrodes. This barrier, known as the Schottky barrier (SB), forms as a consequence of electron energy band offsets across the interface. The magnitude of the Schottky barrier height (SBH) depends on the position of the Fermi level at the interface. Since the perovskite oxides are insulating materials with a relatively small band gap (typically around 3.5 eV), the Schottky emission of electrons into band states is considered as one of the primary sources of leakage in thin perovskite films. In order to reduce the leakage currents and to control the transport properties across the heterojunctions, a thorough understanding of the interface physics down to the atomic scale is crucial.

In this work, we present a systematic theoretical study of the Schottky barriers for a series of transition-metal/$SrTiO_3$(001) (TM/STO) interfaces. STO is a typical representative of oxides with the perovskite structure and serves as an ideal model system for a high-permittivity dielectric material. It is currently used in a variety of integrated devices as a substrate material[3,8,9] but it has been also successfully implemented as an insulating gate in a field-effect transistor.[6] Electrical properties of interfaces between various metals and STO or BST thin films have been studied extensively in the past.[10–25] The experimental studies showed that both the selection of electrode metals and the deposition temperature influence strongly electrical properties. Depending on the electrode material both Ohmic and rectifying Schottky con-

tacts were observed. Even though the SBH were found to correlate with the work function (WF) of the contact metal the reported values are very sensitive to preparation conditions and vary in some cases by more than 1 eV.[24] The only plausible explanation for such a large variation is a dominating role of the interface structure on the SBH.

In order to investigate the underlying mechanisms that govern the SB formation and to examine systematic trends we chose six different transition metals as the electrodes on STO and determined the SBH by first-principles electronic structure calculations. The contact metals were selected from groups VI and X of the periodic table in order to study the possible influence of varying electronic configuration, crystal structure, and atomic size. Additionally, different interface terminations and translations were included in our studies to distinguish between contributions arising from the structural and chemical aspects of the SB formation. Our main goals are to analyze the microscopic quantities, which can be obtained from the first-principles calculations, and relate them to phenomenological models of SBH and experimental measurements.

Furthermore, the present investigation attempts to complement existing theoretical studies of SBH. Previous first-principles calculations have mainly focused on interfaces between metals and either covalent semiconductors (see, e.g., Refs. 26–35) or ionic insulators.[36–39] For many semiconductors the SBH is nearly independent of the metal electrode and the local atomic structures and chemical bonding at the interface is of prime importance. In contrast, interfaces between metals and strongly ionic oxides show a strong dependence of the SBH on the metal contact which stems predominantly from polarization effects of the ionic substrate.[37] The bonding in complex transition-metal oxides exhibits a mixed ionic-covalent character and the interfaces involving the perovskite oxides hence lie between these two extremes. Even though several studies of binary[40,41] and ternary[42–45] transition-metal oxides exist to our knowledge no systematic analysis of the interfaces between TM and perovskite oxides has ever been presented.

The paper is organized as follows. Section II covers the computational first-principles methodology used in our calculations and gives an overview of the investigated systems. In Sec. III we present calculations of separate STO and TM surface systems, which serve as convenient and well-defined references for our study of the TM/STO interfaces. The interface calculations and the theoretical analysis of the SB formation are presented in Sec. IV. In Sec. V we compare results of our first-principles calculations with predictions of existing phenomenological theories of SBH and discuss their similarities and differences. A summary of the work is given in Sec. VI.

II. COMPUTATIONAL METHODOLOGY

A. Mixed-basis pseudopotential method

The Schottky barrier heights were calculated by means of the mixed-basis pseudopotential approach of the density-functional theory (DFT).[46–48] The exchange-correlation contribution to the total energy of DFT was treated in the local-density approximation (LDA).[49,50] Norm-conserving pseudopotentials were used for the description of the core-valence interactions and a mixed basis of localized wave functions and plane waves for the representation of the valence states.[51,52] The pseudopotentials were constructed from all-electron valence-electron states for free atoms following the method of Vanderbilt.[53] Reference configurations different from the free-atom ground-state configurations were used to obtain accurate and transferable pseudopotentials.[54,55] For the representation of the valence-electron eigenstates, localized basis functions with d and p symmetry confined to atom-centered spheres were used for the electrode metals (sphere radii of 1.9 and 1.8 bohr were used for the group X and VI TMs, respectively; 1 bohr=0.529 Å) and for oxygen (radius 1.9 bohr) in STO, respectively. For Ti and Sr in STO, localized functions were included to represent also the outermost core states, i.e., $3s$, $3p$, $3d$ for Ti (radius 1.6 bohr), and $4s$, $4p$ for Sr (radius 1.9 bohr). Plane waves with kinetic energies of up to 20 Ry (1 Ry=13.606 eV) were included in the mixed basis for an accurate description of extended eigenfunctions. The plane-wave cutoff energy was checked to be sufficient for both structure optimizations and analyses of the resulting electronic structures. A discrete sampling with $8\times8\times1$ k points was used for Brillouin-zone integrations in total energy calculations of interface supercells. To account for the metallic character, Gaussian broadening of the eigenvalues by 0.2 eV was used to determine the fractional occupation of the one-electron states in the vicinity of the Fermi level.[52,56] An extensive description of the method and further computational details can be found elsewhere.[46–48,51,52,54,55]

The determination of the SBH was done by analyzing the local electronic structure, using the local (site-projected) densities of states (LDOS) and planar averages of electrostatic potentials (the details of the analysis will be explained later). Calculations of LDOS were performed by projection of one-electron eigenstates onto partial waves in spheres centered at individual atomic sites. For the projection spheres, the Wigner-Seitz radii were used for the six TM and radii of spheres containing formal charges of +2 for Sr, +4 for Ti, and −2 for O in STO.[54,55] The same k-point mesh as in the total energy calculations and Gaussian broadening by 0.1 eV were used to obtain the LDOS results.

B. Supercell models

The TM films on STO substrates were described by supercell models with three-dimensional periodicity. The STO slabs were represented by mirror-symmetrical slabs consisting of seven or nine atomic (002) layers with alternating TiO_2 and SrO planes. The lattice parameters of the supercells parallel to the interface were set to the calculated bulk value of STO (a_{STO}=3.845 Å).[54] The STO (001) surfaces can be terminated either by layers with TiO_2 or SrO compositions. Since both surfaces can be prepared experimentally[8,57] we included both terminations in our study. The TM films with thickness of one, three, or seven (002) atomic planes were then adsorbed on both sides of the STO slabs. The mono- and trilayer systems were studied as free-standing nanoca-

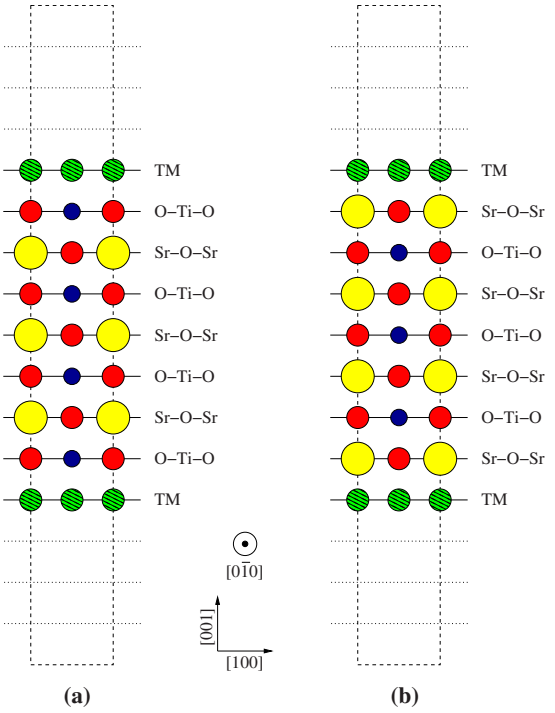

FIG. 1. (Color online) [010] projection of the supercells with seven-layer STO slabs covered on both sides by TM monolayers; (a) TiO_2 and (b) SrO termination.

pacitors separated by a vacuum region. The thickness of the vacuum region was set sufficiently large to avoid spurious interactions between the periodic images of the supercell perpendicular to the metal surfaces. Schematic pictures of the supercells with monolayer metal coverage for the two possible substrate terminations are displayed in Fig. 1.

The investigated electrode metals vary in the equilibrium lattice parameters as well as the equilibrium crystal structures (see Table I). Cr, Mo, and W are group VIB metals with a half-filled *d* band, which crystallize in the body-centered-cubic (bcc) structure. For Ni, Pd and Pt an almost filled d-band leads to stabilization of the close-packed face-centered-cubic (fcc) structure. There are several possible high-symmetry adsorption sites for the TM on both (001) STO surface terminations. This gives a wide range of possible atomic structure models for the TM/STO interfaces. In order to confine the computational burden we selected only the favorable adsorption geometries based on previous theoretical and experimental studies.[8,42,54,58–61]

TABLE I. Calculated equilibrium lattice parameters a_{TM} and the lattice mismatch between the metals and STO (a_{STO}=3.845 Å). The values in brackets correspond to the interatomic distance along the bcc ⟨110⟩ direction (i.e., $\sqrt{2}a_{TM}$) which lies parallel to the STO ⟨100⟩ direction for the bcc-TM/STO interfaces.

Metal	a_{TM} (Å)	Lattice mismatch (%)
Cr	2.81 (3.97)	+3.4
Mo	3.14 (4.44)	+15.6
W	3.14 (4.44)	+15.6
Ni	3.45	−10.1
Pd	3.88	+0.9
Pt	3.93	+2.2

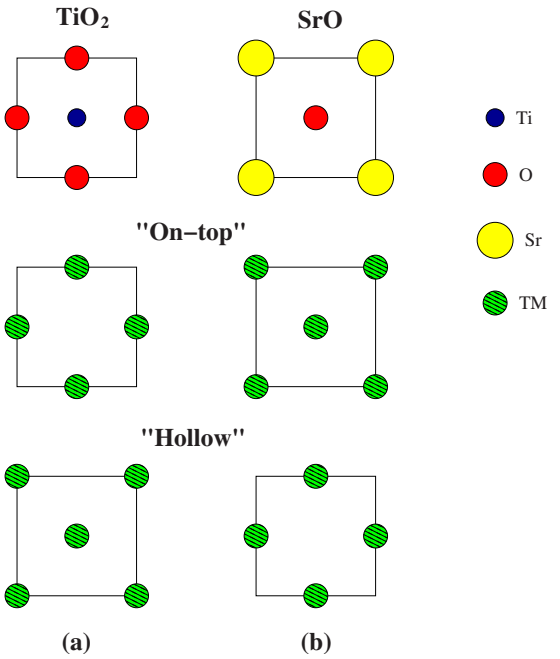

FIG. 2. (Color online) [001] view of the on-top and hollow arrangements of the TM layers on the (a) TiO_2- and (b) SrO-terminated (001)STO surfaces.

Several TM/STO interfaces have been studied by DFT methods in the past. The atomic and electronic structures of the Pd/STO and Mo/STO interfaces have been investigated in detail in our group.[54,58,59] These studies predict that the preferred adsorption sites of metal atoms for the TiO_2 surface are on top of oxygen atoms while for the SrO surface they are on top of oxygen and strontium atoms. In a similar study of the Pt/STO interface, Asthagiri *et al.*[60] found that Pt prefers to bind on top of oxygen atoms on both terminations. Rao *et al.*[42] obtained equivalent results for BaO-terminated (001) surface of barium titanate with several transition-metal elements. These theoretical predictions were also confirmed experimentally in recent electron microscopy studies.[8,61,62] Based on this extensive evidence, we consider the "on-top" position as the favorable absorption site for all TM elements chosen in this study.

In order to examine the influence of interface geometry on the SBH we investigated for some metals also another arrangement, where the metal atoms are positioned on top of the fourfold hollow sites of the STO surface. These configurations have significantly lower binding energies than the on-top sites[54,60] but may occur, for example, at interfacial defects such as the cores of misfit dislocations.

The investigated adsorption geometries are schematically shown in Fig. 2. In both arrangements there are two TM atoms per surface unit cell, which corresponds to a monolayer coverage of the substrate. The orientation of the metal layer in the case of the fcc metals films is such that the (100) planes and ⟨100⟩ directions in both materials are parallel to

each other, i.e., the metal exhibits the so-called cube-on-cube epitaxy with the substrate. In the case of bcc metals, the (100) planes are again parallel in both materials but the metal lattice is rotated by 45° so that the ⟨100⟩ direction in STO is parallel to the ⟨110⟩ direction in the TM.

As will be discussed later the relaxation has a strong influence on the electronic structure of the interfaces and is therefore of crucial importance for a reliable determination of SBH. All interfaces were optimized by relaxing the forces on all atoms to values smaller than 0.02 eV/Å. This limit was found sufficient as our test calculations showed that lowering of the tolerance to 0.005 eV/Å does not influence the results.

III. SURFACE CALCULATIONS

Separate TM and STO materials with defect-free surfaces present a natural starting point for studies of the TM/STO interfaces and can serve as convenient and well-defined reference configurations. Before we proceed to the interface calculations we therefore focus first on the key properties of the constituting materials that are related to the SBH. These characteristic properties are the work function of the metal, and the ionization potential and electron affinity of the insulator. Since all these quantities depend sensitively on the atomic and electronic structures of surfaces we discuss in this section available theoretical predictions and experimental observations of the investigated TM and STO surfaces.

A. Transition metals

One of the most important properties of a metal surface is its WF. It corresponds to a potential difference between the Fermi energy and the vacuum level and depends on the surface dipole that forms due to a spilling of electrons into the vacuum. It is also the only material parameter characterizing the metallic electrode in empirical theories that are used for estimating the SBH.[63]

First-principles DFT calculations of work functions are nowadays routinely carried out using a sufficiently thick metallic slab embedded in a vacuum region. Several systematic studies[64–69] have demonstrated the ability of DFT to give reliable values of work functions that agree closely with experimental data. Our calculated WFs are presented in Table II. The second column contains results calculated for the equilibrium lattice constants of each TM whereas the results in the third column were obtained with the lateral lattice parameter fixed to the equilibrium lattice constant of bulk STO. In all calculations the atomic positions were relaxed. As expected, for metals with a small lattice mismatch to STO (i.e., Cr, Pd, and Pt) the work functions in the second and third columns of Table II are almost the same. For the remaining three metals, the lattice straining has a strong influence on the work function. As shown in Table I the equilibrium lattice constants of Mo and W are almost 16% larger than that of STO and the work functions of these two metals in the third column of Table II correspond to a state of strong lateral compression. Under such conditions, the so-called Smoluchowski smearing[76] parallel to the surface is reduced while the spread of electrons into the vacuum is enhanced causing an increase in the surface dipole and hence an increase in the work function. An opposite effect happens for Ni, which has a smaller lattice parameter than STO. The lattice expansion leads to better smoothing of the surface charge density and a lowering of the work function. Altogether, our calculated WF values agree very well with available theoretical as well as experimental data. Especially the agreement with the recommended estimates of the work function for clean monocrystalline surfaces from a very recent extensive compilation of Kawano[73] is very good with the only exception of Pt, whose calculated work function slightly overestimates the experimental value.

TABLE II. Calculated and experimental work functions (WF) for the TM in this study; the third column contains values calculated with the lateral lattice parameter equal to the lattice parameter of STO.

	This work			
	a_{TM}	a_{STO}	Theory	Experiment
Cr	4.50	4.57	4.48[a]	4.50,[b] 4.46[c]
Mo	4.40	4.84	4.05[d]	4.53,[b] 4.40 ± 0.03[e]
W	4.54	5.00	4.63[f]	4.63,[b] 4.57 ± 0.03[e]
Ni	5.29	5.05	5.31[g]	5.22,[b] 5.23 ± 0.10[e]
Pd	5.50	5.54	5.30,[d] 5.96[h]	5.65,[i] 5.59 ± 0.05[e]
Pt	6.09	6.08	6.97,[h] 6.20[j]	5.65,[b] 5.82 ± 0.07[e]

[a]Reference 70.
[b]Reference 71.
[c]Reference 72.
[d]Reference 64.
[e]Reference 73.
[f]Reference 65.
[g]Reference 74.
[h]Reference 66.
[i]Reference 75.
[j]Reference 67.

B. STO

Since STO is a prominent perovskite representative, the atomic and electronic structures of its surfaces have been studied extensively in the past, both theoretically and experimentally. Surprisingly, even though the number of studies is large, the understanding of STO surface structures is still far from being complete.[9,77–83] The reason is a large variability of possible surface reconstructions, transformations, and formations of nanostructures, which depend sensitively on processing (e.g., reducing or oxidizing) conditions.

In the present work, it is not our aim to contribute to the issues of stability and structure of STO surfaces. We assume that our systems are built from ideal, atomically sharp (001)-type surfaces with either SrO or TiO_2 terminations. It has been shown in a detailed comparative study[84,85] that both DFT (with various exchange-correlation functionals) and Hartree-Fock calculations of the (001) STO surfaces provide consistent results for surface rumplings and relative displacements of the surface planes. Our calculations of surface structures and atomic displacements for relaxed 7-, 9-, and 11-layer slabs agree well with the previous DFT studies[84–89] and therefore we need not discuss them here.

The main reason why we carried out the surface calculations was to obtain a clear comparison of the atomic and electronic structures at the clean STO surfaces with those at the TM/STO interfaces. Like in the case of metal surfaces described in the previous section, we are mainly interested in quantities that are related to the band alignment at interfaces and the formation of the Schottky barrier. In the following we will therefore focus on the determination of the work function, ionization potential (IP), and electron affinity (EA) for the STO surfaces with the two (001) terminations.

The analysis of the surface electronic structure and the determination of the characteristic band positions with respect to the vacuum level in DFT calculations can be obtained using three well-established approaches: alignment of the atomic core levels,[90] macroscopic averaging (MA) of the electrostatic potential,[91,92] and analysis of the local densities of electronic states. Because we employ pseudopotentials in our calculations we are able to carry out only the last two analyses. Previous studies however showed that all three methods usually agree within 0.1–0.2 eV for well converged calculations and appropriate system sizes (see, e.g., Refs. 32, 37, and 93).

Before we discuss the results of the two analyses we would like to provide a clear definition of the quantities that can be extracted from the calculations. Some caution is especially needed when referring to the work function and the ionization potential, as the use of these two terms for insulating materials is somewhat ambiguous. Moreover, the correspondence between computed and measured quantities is usually not straightforward, which may lead to inappropriate comparisons (for a more detailed discussion of this subject see Refs. 94–97).

The ionization potential is defined as the energy difference between the valence-band maximum *deep inside the solid* and the vacuum level just outside the surface (i.e., at a distance large compared to atomic dimensions but smaller than macroscopic dimensions of the surface[97]). The expression "inside the solid" in first-principles calculations means far enough from the surface (or interface) for microscopic quantities to recover their bulk features. It however does not correspond to macroscopic dimensions where other effects, such as band bending due to a space charge zone, occur. Within this definition the IP is different for different surface orientations (such as the WF), since it depends on the surface dipole, but it is not directly determined by surface states that may arise due to broken bonds.

The work function is a property that is determined by the position of the Fermi level E_F (the chemical potential of electrons at zero temperature), which is constant within the whole material. While in an ideal insulator E_F lies in the middle of the band gap, in real materials it depends on the experimental conditions, stoichiometry deviations, surface adsorbates, dopants or impurities, as well as on changes in the surface electronic structure. Dangling bonds may even lead to surface metallicity and Fermi level pinning by the surface states. For our ideal STO slabs all extrinsic effects are excluded. The Fermi level in our calculations corresponds to the energy of the highest occupied state and the calculated work function thus presents a theoretical upper limit for ideal STO surfaces. As we will see below, E_F differs significantly from the IP only for the TiO_2-terminated surface, which contains surface states that protrude into the band gap.

While the ionization potential is the energy needed to bring the electron from the top of the valence band to the vacuum, its close relative, the electron affinity, is the energy difference between the vacuum level and the conduction-band minimum inside the solid. The difference between the two quantities in insulators is equal to the width of the band gap. The slab calculations can in principle provide the electron affinity, which is often used in empirical theories of SBH.[63] Here we are however confronted with the well-known underestimation of the band gap in DFT calculations related to the inability of DFT to describe properly the unoccupied states. A usual way to cure this problem is to use an experimental value for the band gap [3.3 eV for STO (Ref. 98)].

Apart from the band-gap problem, common DFT calculations suffer from the approximative treatment of exchange correlation, which neither the LDA nor generalized-gradient approximations describe correctly. More accurate treatments of many-body effects (e.g., GW approximation or self-interaction correction) are computationally more demanding and do not necessarily provide better results (for instance, recent GW calculations of Cappellini *et al.*[99] overestimate the band gap of STO by 2 eV). It is therefore rather difficult to estimate the error of LDA in determining the IP and EA in STO. Considering that corrections of about 1.0 eV and 0.2–0.4 eV were reported for wide-band insulator MgO (Ref. 37) and semiconducting Si (Ref. 95) and GaAs,[100] respectively, we can assume that similar corrections of the order of several tenths of eV may apply also for STO. A more detailed assessment of systematic errors and a comparison with available experimental data will be given below.

The electronic structure of the STO surface slabs in terms of the local densities of states is depicted in Fig. 3. Since the upper valence band in STO consists mainly of oxygen $2p$ states[86,98] we show only the oxygen LDOS as they vary from the surface layer (top) to the central layer (bottom) in the nine-layer STO slab. The figure contains also the LDOS of oxygen atom from ideal bulk STO in shaded gray for comparison.

The sequence of LDOS graphs in Fig. 3 provides us with a real-space picture of the electronic structure. It shows that the electronic states near the surface are different from those in the bulk. The influence of surfaces however decays quickly, and already in the third plane below the surface the LDOS resembles closely that of the bulk.

The LDOS graphs confirm that both surfaces remain insulating; a fact that has been known experimentally for a long time.[101,102] Besides this common feature, the surface electronic structures of the two surface terminations exhibit markedly different characters, as was noted in earlier studies.[78,85–87,103] The valence-band maximum (VBM) in the SrO-terminated slab is determined by the states on the central "bulklike" oxygen atoms while the width of the valence band at the surface is slightly reduced. This feature is visible on the uppermost LDOS in Fig. 3(a). Since there are no salient states due to dangling bonds present in the gap this surface rather resembles surfaces of typical ionic compounds

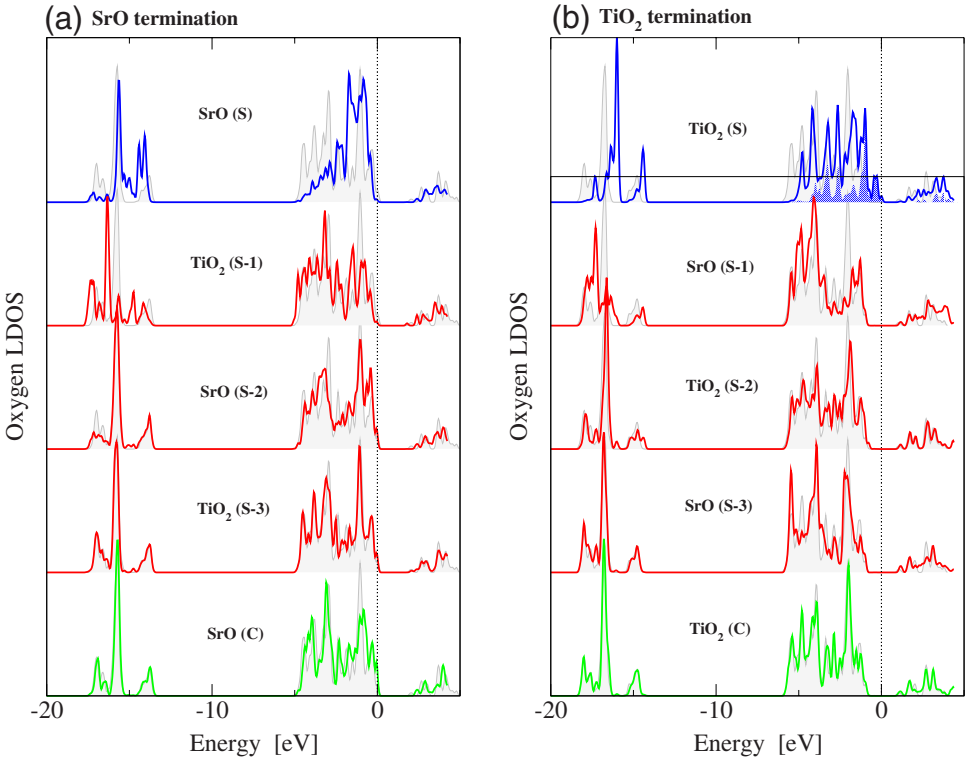

FIG. 3. (Color online) Calculated LDOS for the surface and central oxygen atoms from relaxed (a) SrO-terminated and (b) TiO_2-terminated nine-layer STO slabs. All panels contain also the LDOS of oxygen from bulk STO in shaded gray for comparison (the bulk curves are rigidly shifted by the same amount to match the LDOS of the central oxygen). The zero energy corresponds to the Fermi level of the slabs.

(e.g., SrO) that are formed without breaking of covalent bonds or large charge redistributions.[104] In contrast, the TiO_2-terminated surface exhibits a split at the top of the valence band of the surface oxygen atoms and a formation of new surface states that intrude into the gap and decrease its width. These states are composed of lone-pair oxygen $2p$ orbitals that lie perpendicularly to the Ti-O-Ti bonds in the surface plane [these states are shaded in dark gray (blue) in the uppermost LDOS in Fig. 3(b)]. The position of the highest occupied level for the TiO_2-terminated surface is then determined by these surface states while the VBM in the central bulk part of the crystal is positioned about 0.9 eV lower.

The LDOS curves thus allow us to distinguish between the VBM of the bulk material and VBM of the surface region. It is clear that these two quantities are different in the two terminations and their correct determination is important for the analysis of the band alignment at interfaces.

The macroscopic averaging of the electrostatic potential provides a complementary view to the LDOS analysis. This well-established "nanosmoothing" procedure[105] is nowadays often used for determination of band offsets at interfaces but it can be applied as well to obtain the work function and ionization potential in surface slab calculations.

The planar and macroscopic averages of the electrostatic potential for ideal unrelaxed and relaxed STO surfaces are displayed in Fig. 4. The STO ionization potential I_S is determined within the MA approach as

$$I_S = \Delta V - E_{\text{bulk}}^{\text{VBM}} = (E_{\text{vac}} - \bar{\bar{V}}_{\text{central}}) - E_{\text{bulk}}^{\text{VBM}}, \qquad (1)$$

where $E_{\text{bulk}}^{\text{VBM}}$ is the STO valence-band maximum referenced with respect to the average electrostatic potential in the bulk material. ΔV is the difference between the vacuum level and the average of the electrostatic potential in the center of the slab from the slab calculation. The vacuum level E_{vac} in all graphs corresponds to zero energy while the bulk term $E_{\text{bulk}}^{\text{VBM}}$ in our calculations equals 5.08 eV.

In agreement with the LDOS analysis, the bulk VBM and the Fermi level from the MA analysis almost coincide for the SrO-terminated surface and, according to our consideration above, the WF and IP are therefore equivalent. A small difference of about 0.1 eV arises due to finite k-point mesh, slab size, and fluctuations in the macroscopic average. These factors determine the overall accuracy of the determined values. For the TiO_2-terminated surface the MA and LDOS results are also consistent. The Fermi level (the energy of the highest occupied state) is determined for this termination by the surface states and lies 0.82 eV (MA) compared to 0.93 eV (LDOS) above the bulk VBM. The small difference is again within the expected systematic error margins.

The calculated values of ionization potentials, work functions, and electron affinities for the STO surfaces are listed in Table III. We see that the IP increases with surface relaxation for both terminations. This is plausible since the shifts of atoms from their ideal bulk positions lead to an increase in the surface dipole, which is directly related to the IP. Interestingly, the IP is significantly larger for the TiO_2 termination than for the SrO termination pointing to a large difference in the surface dipole moments between the two surfaces. Our results agree qualitatively but not quantitatively with those of a DFT study of Cheng *et al.*[89] who obtained only about 13% difference between the surface dipole moments of the two terminations. These authors however determined the dipole moment from the step of the electrostatic potential ΔV and a simple asymptotic $(1/r)$ form of the electron-ion potential. The reported values are therefore only approximate. We

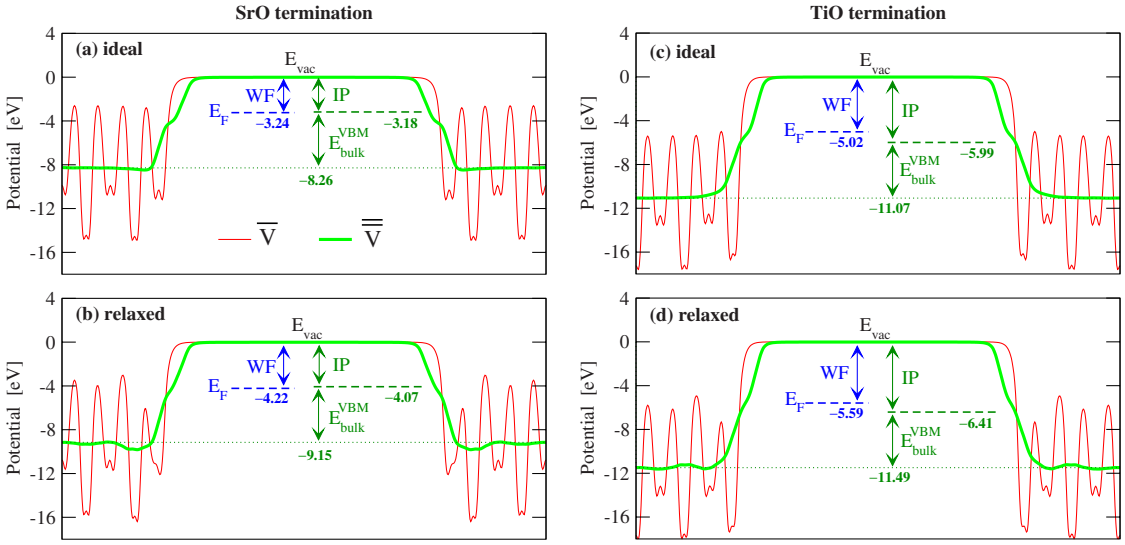

FIG. 4. (Color online) Planar averages $\bar{V}$ and macroscopic averages $\bar{\bar{V}}$ of the electrostatic potential for (a,c) ideal and (b,d) relaxed SrO- and TiO_2-terminated surfaces of STO, respectively.

would like to emphasize here that ΔV has no physical meaning as the partition in Eq. (1) is not unique and depends on the assumptions made to fix the arbitrary constant in the electrostatic potential (e.g., ΔV depends on the employed pseudopotentials). The same is true when the MA approach is used for the determination of band offsets and Schottky barriers at interfaces.[106–108] The only physically meaningful quantities in Eq. (1) are either the IP or changes in ΔV, for instance, upon relaxation. We will return to this subject in more detail in the next section when discussing the interface dipole.

To our knowledge, there exist only few experimental data for WF, IP, and EA of STO, most of them for an Nb-doped (*n*-type) material. Due to the *n*-type doping the Fermi level lies close to the bottom of the conduction band and the measured work functions then roughly coincide with the electron affinity. Chung and Weissbard[102] measured WF of 4.2 eV for the *n*-type (001) STO surface using ultraviolet photoemission spectroscopy (UPS). Henrich *et al.*,[101] however, showed that the work function varies substantially with different surface conditions, namely, oxygen content and concentration of surface defects. More recently, Moller *et al.*[109] obtained a value of 4.1 ± 0.1 eV for a (2×2) reconstructed (oxygen deficient) surface. After adding the experimental band-gap width, these values correspond to IP of about 7.5 eV. A significantly lower WF (again coinciding with EA) of 2.6 eV for the TiO_2-terminated surface of undoped STO was found by Maus-Friedrichs *et al.*[110] using UPS (HeI) and metastable impact electron spectroscopy who also determined the position of the VBM to be 5.7 ± 0.2 eV below the vacuum level. In a most recent *in situ* photoemission study Schafranek and Klein[23] reported a variation in the WF between 4 and 4.7 eV and IP of 7.4 ± 0.1 eV for the *n*-type STO.

TABLE III. Calculated ionization potentials IP, work functions WF, and electron affinities EA (values obtained with experimental band gap are in brackets) of STO surfaces (all values are in eV).

	Ideal		Relaxed	
	SrO	TiO_2	SrO	TiO_2
IP	3.18	5.99	4.07	6.41
WF	3.24	5.02	4.22	5.59
EA	1.25 (−0.12)	4.06 (2.69)	2.14 (0.77)	4.48 (3.11)

Theoretically, Piskunov *et al.*[103] determined the VBM position of the TiO_2-terminated surface 5.9 eV below the vacuum level using a DFT approach with a hybrid exchange-correlation functional that is claimed to provide the most reliable band gaps for perovskite oxides. It is important to note that the VBM in this study was determined from the highest occupied surface state and the value thus should be compared to the work function in our calculations. As their reported band-gap reduction due to the surface states amounts to about 0.5 eV, the corresponding IP, i.e., with respect to VBM in the crystal interior, equals to 6.4 eV. These results agree very well with our LDA predictions of 5.6 eV (WF) and 6.4 eV (IP) for this surface (see Table III). Hence, it appears that the choice of the approximate exchange-correlation functional does not affect critically the position of the highest occupied levels with respect to the vacuum level.

The comparison of all available theoretical and experimental data unfortunately does not provide a consistent picture about the position of band edges at STO surfaces. The theoretical predictions of IP are supported only by the experiment of Maus-Friedrichs *et al.*[110] whereas much larger values (by almost 2 eV) are reported from all other observations. It is clear that the scatter of reported experimental data is rather large, and that the published results seem to depend sensitively on the surface structure, doping level, as well as experimental preparation technique. Systematic errors in theoretical calculations due to many-body effects are also likely

to be present; their magnitude is however still uncertain. Obviously, more surface studies are required by both experiment and theory before final conclusions can be obtained.

IV. INTERFACE CALCULATIONS

The surface calculations presented in the previous section provide us with information on the reference systems—the relaxed (001) TM surfaces and the relaxed SrO- or TiO_2-terminated (001) STO slabs. A comparison of the metal work functions in Table II with the theoretical ionization potentials of the two relaxed STO surfaces in Table III gives us a first indication that the two terminations are likely to behave differently during interface formation. Whereas the TM work functions range from 4.5 to 6 eV, the SrO-terminated STO surface has its VBM only 4 eV below the vacuum level. The Fermi levels of all investigated TM hence lie below the VBM of STO. Thus charge transfer and formation of a dipole layer at the interface is necessary to move the metal Fermi level inside the insulator band gap in order to achieve the spatial uniformity of the chemical potential in the whole system. This result is clearly incompatible with the Schottky-Mott model that assumes no interaction between the materials constituting the interface.[63] The situation is opposite for the TiO_2-terminated STO surface. Its ionization potential of 6.4 eV is larger than the work functions of all investigated metals and their Fermi levels thus lie within the STO band gap even before the materials are rigidly joined. In this case the Schottky-Mott model can be applied for an estimation of the SBH.

In reality the formation of interfaces between transition metals and perovskite oxides is associated with a creation of new chemical bonds and substantial rearrangements of the electron density. Additionally, the atomic positions in the vicinity of the interface are usually significantly altered to minimize the total energy of the system. Both of these processes contribute to the final charge distribution and alignment of the energy levels at the interface. While during experimental interface formation these two processes happen simultaneously and it is impossible to separate the two contributions, theoretical modeling gives us the freedom to study them individually.

In order to analyze the atomic and electronic relaxations independently we decided to dissect the process of interface formation into three stages, which are shown schematically in Fig. 5. As a starting point (stage 0) we consider separate and appropriately oriented and terminated STO and TM slabs whose surfaces have been relaxed to their equilibrium configurations (here we expect for simplicity that the metals already adopt the lateral lattice parameter of STO). In a first step, while still kept apart, the surface structure of both materials is transformed to a configuration that the materials would adopt at the relaxed interface. We call this stage "atomic rearrangement." In the second stage the two materials are brought rigidly together to a distance corresponding to the equilibrium interface separation. Since the atoms in both materials are already fixed at their "interfacelike" equilibrium positions, only the electronic degrees of freedom need to be relaxed at this step to minimize the interface energy. We call the second stage accordingly "electronic rearrangement."[111]

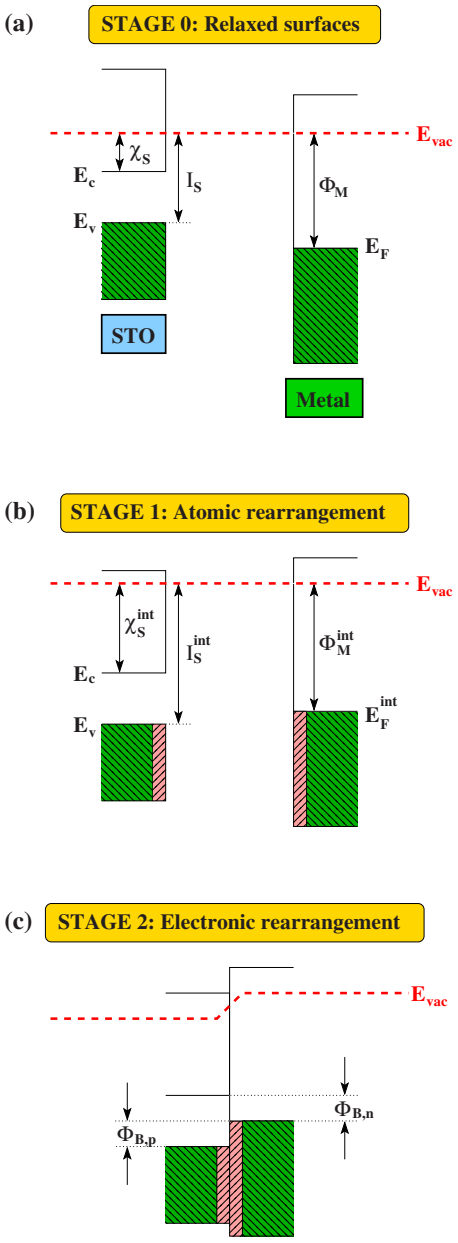

FIG. 5. (Color online) Schematic picture of energy band diagrams corresponding to three stages of interface formation used in the analysis of SBH. In stage 0, appropriately oriented and terminated relaxed STO and TM slabs present an initial reference configuration. In stage 1, the materials remain separated but the atomic positions are rearranged as if a fully relaxed interface were formed. In stage 2, the slabs are brought together to form the interface; the electronic density changes due to formation of new chemical bonds across the interface but the atomic positions in both slabs remain the same.

The main advantage of this procedure is a possibility to identify better the physical mechanisms that are dominating for the lineup of bands at the interface. In particular, the step-by-step process of interface formation allows us to separate the changes due to atomic and electronic relaxations at the interfaces. With the relaxed surfaces as reference states

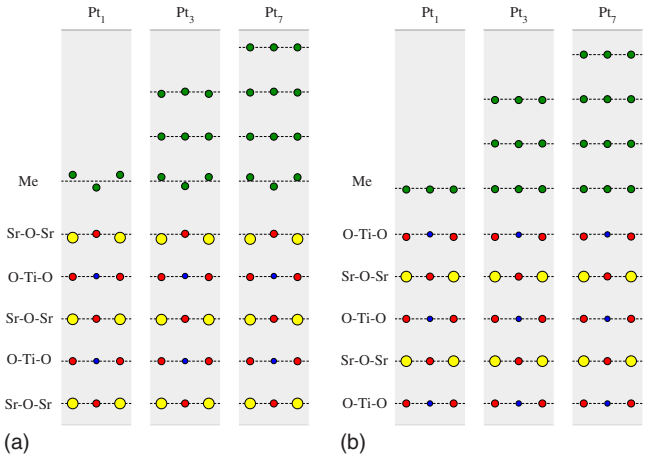

FIG. 6. (Color online) Side [010] view of relaxed (a) SrO-terminated and (b) TiO_2-terminated Pt/STO supercells with different metal coverages (only one half of the symmetric supercells are shown).

we can partly circumvent the ambiguities in the definition of the key quantities of interest—the interface charge (monopole) and dipole densities—which are the main attributes in the determination of the SBH.[105]

A. Pt/STO system

We start our investigation of the SBH with a thorough examination of the Pt/STO system. On this system we test the procedure described above and analyze the interfacial properties related to SBH. The stability, structure, and electronic characteristics of various Pt/STO interfaces have been studied by Asthagiri and Sholl.[60,112,113] These studies identified the on-top positions of metal atoms above the oxygen sites to be the preferred adsorption sites. We therefore limit our test calculations to these configurations.

In order to investigate the influence of metal coverage the calculations were carried out for three different thicknesses of the Pt layers. The first supercell contained alternating STO and Pt slabs (with seven metal layers) periodically repeated without any vacuum region. In the remaining two supercells tri- and monolayer Pt films were deposited on both STO surfaces and these nanoscale capacitors were separated by a vacuum region that was sufficiently large to avoid the interaction between the metal surfaces in periodically repeated images. Figure 6 shows relaxed atomic positions in these three types of supercells. It is obvious even without quantitative examination that the interfacial structure is very similar in all three systems and already the monolayer coverage invokes similar atomic relaxations at the interface as in the limiting seven-layer bulklike case.

As already shown in the previous section on STO surfaces, first-principles calculations provide several ways of how to determine the relative positions of energy levels on both sides of the interface. In the multilayer supercells the widths of the STO (nine layers) and metal (seven layers) slabs are large enough for microscopic quantities to recover their bulk features in the central regions of the slabs. Thus in this system the difference between the VBM in the bulk

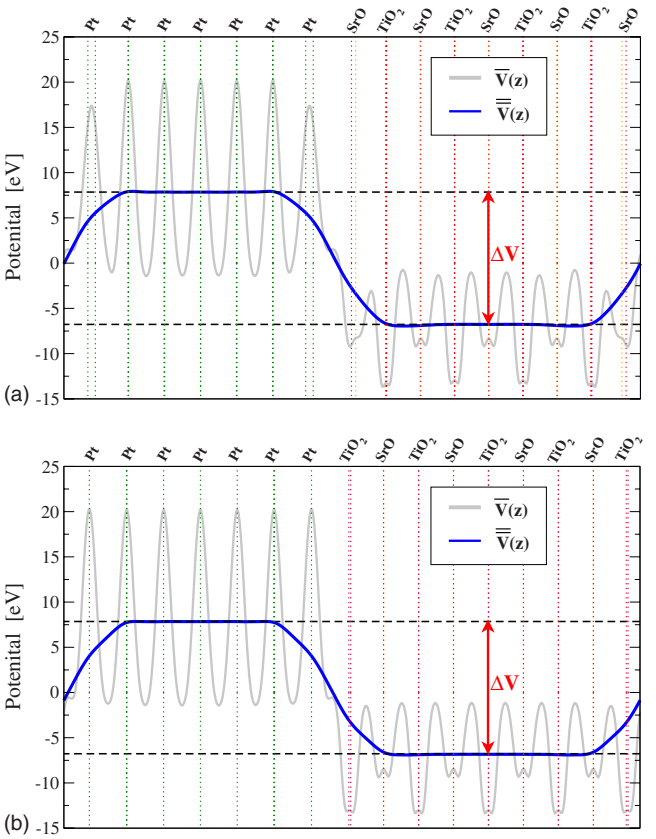

FIG. 7. (Color online) Planar and macroscopic averages of the electrostatic potential in the (a) SrO-terminated and (b) TiO_2-terminated Pt/STO system. The dotted vertical lines mark the positions of atomic planes.

part of STO and the Fermi level, which is equal to the p-type SBH $\Phi_{B,p}$, can be easily obtained using the MA approach.[91,92]

Similarly like the IP in surface calculations, the p-type SBH is determined within the MA approach as

$$\Phi_{B,p} = \Delta E_{\text{bulk}} + \Delta V, \tag{2}$$

where ΔE_{bulk}, often called the "band-structure term," is obtained from independent bulk calculations for each material.[91,92] In our case this term is a difference between the Fermi level of the metal and the VBM of STO, each measured with respect to the average electrostatic potential of the corresponding bulk crystal. The second term ΔV is the difference between the average electrostatic potential in the two materials far from the interface obtained from the interface supercell calculation. We again emphasize here that even though the potential shift ΔV is sometimes associated with the interfacial dipole it has no physical meaning.[91,92,107,108] An example of the planar and macroscopic averages of the electrostatic potential in the Pt/STO system obtained from our calculations is shown in Fig. 7.

For the supercells with mono- and trilayer Pt coverage the MA technique cannot be used because the macroscopic averages for such thin slabs are inaccurate. An alternative way for the determination of SBH is the LDOS analysis.[106] In the LDOS method the valence-band edge of STO can be directly

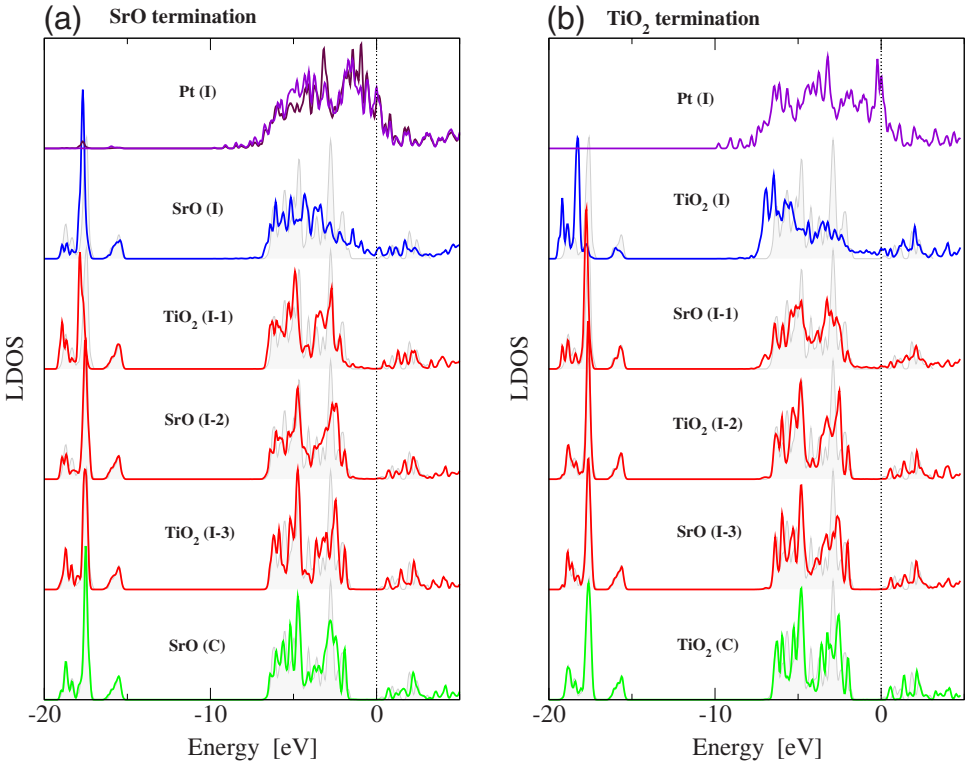

FIG. 8. (Color online) Sequence of LDOS in the (a) SrO-terminated and (b) TiO_2-terminated Pt/STO system. The zero energy corresponds to the Fermi level.

obtained from the oxygen LDOS of the central layer in the slab. The SBH $\Phi_{B,p}$ is then simply the difference between this VBM and the Fermi level which is computed accurately by DFT calculations. A sequence of LDOS curves from the multilayer Pt/STO system is plotted in Fig. 8. A significant hybridization between the Pt 5*d* and O 2*p* states at the interface is apparent. The interface-induced changes in the electronic structure are mainly concentrated in the interfacial region. Some small perturbations are still visible at the valence band of the central oxygen atom, so even at relatively large distances from the interface the bulk features are not completely recovered.

A disadvantage of the LDOS analysis is an uncertainty in locating precisely the VBM due to *k*-point sampling, Gaussian smearing, and small but still discernible effects of the interface in the center of the supercell. This uncertainty, which may reach few tenths of electron volts, can be removed by combining the LDOS analysis with a procedure related to the alignment of core levels.[90] Specifically, we can line up the LDOS of the central oxygen atom in the slab with the oxygen LDOS from bulk STO. Since there are no core levels in our pseudopotential calculations, this level matching (denoted further as LM) is done for the semicore O 2*s* states between −20 and −15 eV (see Fig. 8). After the two LDOS curves are aligned the VBM corresponds to the highest occupied level in the bulk LDOS, which is known with a high precision. It is clear from Fig. 8 that even though the bulk oxygen LDOS matches closely with the central oxygen LDOS from the interface calculation there are still noticeable differences. It is interesting to note that the bulk oxygen LDOS matches better with the oxygen LDOS from the innermost TiO_2 layer than from the innermost SrO layer even if the SrO layer is the central layer in the slab.

Calculated SBH values $\Phi_{B,p}$ for all Pt/STO interfaces determined by the three methods are summarized in Table IV. All methods yield consistent results with differences not exceeding 0.1 eV, which is an expectable result for well converged calculations. Interestingly, the SBH for both terminations and all metal coverages are very similar, as to be expected in the case of strong pinning (Bardeen limit). We will see in the next section that this is not true in general for the TM/STO interfaces.

Before we examine in detail various aspects of the SB formation we compare the results of our calculations for the Pt/STO interface to other theoretical predictions and experimental measurements. In a recent publication Schafranek *et al.*[24] presented a detailed photoemission study of the SBH for various $(Ba,Sr)TiO_3/Pt$ interfaces and compared carefully all experimental and theoretical data available for this sys-

TABLE IV. Values of the *p*-type SBH ($\Phi_{B,p}=E_F-\mathrm{VBM}$) in the Pt/STO system determined by different methods (all values are in eV).

	MA	LDOS	LM	Eq. (3)
SrO term				
7 Pt	1.73	1.78	1.72	1.74
3 Pt		1.71	1.65	1.62
1 Pt		1.72	1.72	1.74
TiO_2 term				
7 Pt	1.78	1.86	1.83	1.77
3 Pt		1.84	1.80	1.79
1 Pt		1.81	1.76	1.75

tem. Their compilation shows that the experimentally determined SBH for electrons vary considerably ($\Phi_{B,n}^{\mathrm{exp}}$ =0.4–1.6 eV) and the measured values depend sensitively on sample preparation and experimental conditions like for the STO surfaces. It seems that the most critical issue for the SBH is the oxygen content. For interfaces prepared under reducing conditions, which likely contain a large number of oxygen vacancies, much smaller SBH for electrons are observed than for fully oxidized interfaces. Schafranek *et al.*[24] determined the electron SBH for the defect-free Pt/STO interface to be between 1.3 and 1.5 eV, which translates to the hole SBH $\Phi_{B,p}^{\mathrm{exp}}$=1.7–1.9 eV when the experimental value of the band gap is subtracted. This range agrees perfectly with our theoretical predictions in Table IV. In another DFT study Rao *et al.*[42] obtained a much smaller $\Phi_{B,p}$ of 0.96 for the BaO-terminated Pt/BTO interface. However, their calculations were done for a half monolayer coverage, i.e., Pt atoms only above the oxygen sites of the surface (cf. Fig. 1). The results of this study thus cannot be directly compared to results of our calculations or experiments since it is very likely that such a low metal coverage will not lead to the same SBH as the thicker films.

We would like to mention here only briefly that an empirical estimation of 0.89 eV for the electronic SBH by Robertson and Chen[114,115] fits within the wide range of experimental data but is significantly smaller than the predictions for the defect-free interface. We will discuss in more detail the relation between the results of first-principles and empirical methods in Sec. V.

B. Theoretical analysis of Schottky-barrier formation

While it is relatively straightforward to obtain the magnitude of the SBH from first-principles calculations, it is much more valuable to analyze the most relevant quantities that determine the band lineup at the interface. Following the three stages of interface formation described in the beginning of this section, we can decompose the total SBH $\Phi_{B,p}$ into three contributions as

$$\Phi_{B,p} = \Phi_{B,p}^{(0)} + \Delta\Phi_{B,p}^{(1)} + \Delta\Phi_{B,p}^{(2)}. \tag{3}$$

The three terms correspond to the three stages of interface formation displayed in Fig. 5. The first term on the right-hand side of Eq. (3), $\Phi_{B,p}^{(0)}$, is the ideal SBH in the Schottky-Mott limit, which is simply the difference between the ionization potential of STO (cf. Table III) and the work function of Pt (cf. Table II):

$$\Phi_{B,p}^{(0)} = I_S - \phi_M. \tag{4}$$

The other two terms in Eq. (3), $\Delta\Phi_{B,p}^{(1)}$ and $\Delta\Phi_{B,p}^{(2)}$, can be understood as corrections to this ideal model and represent the changes in the SBH due to atomic and electronic rearrangements at the interface, respectively. The relaxation-induced change can be further split into

$$\Delta\Phi_{B,p}^{(1)} = \Delta I_S^{(1)} - \Delta\phi_M^{(1)}, \tag{5}$$

where $\Delta I_S^{(1)}$ and $\Delta\phi_M^{(1)}$ are the shifts of the STO ionization potential and metal work function, respectively, when the atomic structures of the surfaces are transformed in step 1 from their equilibrium to the interfacelike configurations. The changes in IP and WF in this step are therefore related solely to the modifications of the surface dipoles. Finally, the electronic relaxation during the interface formation in step 2 is associated with an electron density redistribution that minimizes the interfacial energy and equalizes the Fermi level in the whole system. This process usually results in electrons being transferred across the interface and leads thus to the creation of an interfacial dipole, which induces a step $\Delta V^{(2)}$ in the electrostatic potential at the interface. Within our procedure this potential shift can be extracted by subtracting the superimposed planar or macroscopically averaged electrostatic potentials of the interfacelike Pt and STO slabs (obtained in step 1) from the planar or macroscopically averaged potential of the relaxed Pt/STO interface (obtained in step 2). In this derivation $\Delta V^{(2)}$ presents a change in the electrostatic potential across the interface. The correction of the SBH due to the electronic rearrangement is then expressed as

$$\Delta\Phi_{B,p}^{(2)} = \Delta V^{(2)} - \Delta\phi_M^{(2)}, \tag{6}$$

where $\Delta\phi_M^{(2)} = \phi_M^{(2)} - \phi_M^{(1)}$ is again a change in the metal work function corresponding to the shift of the Fermi level. The term $\phi_M^{(2)}$ is also known as the effective work function $\phi_{M,\mathrm{eff}}$.[116] We will return to this quantity, characterizing the work function of a metal attached to a substrate, in more detail in the next section.

All quantities that enter Eqs. (3)–(6) are summarized for the Pt/STO interfaces in Table V. Pt has the largest work function of all investigated metals, which results in negative (i.e., unphysical) or very small values of the ideal SBH. This implies that significant atomic and electronic reorganization has to take place when the two materials are joined together to equalize the Fermi level in the whole system.

The data in Table V show that the transformation of the equilibrium surface structures into the interfacelike configurations (step 1) has almost no effect on the metal work functions and changes only slightly the IP for the SrO-terminated surfaces. The large and negative values of $\Delta\Phi_{B,p}^{(1)}$ for the TiO_2-terminated surfaces on the other hand cause the VBM of STO to shift above the Fermi level of Pt. The ideal SBH (in the Schottky-Mott limit) of such a system would be therefore negative as for the SrO-terminated surfaces. The interface-induced atomic relaxation in this particular case thus does influence significantly the band lineup but acts in the unexpected direction leading to a thermodynamically unstable system.

The equalization of the Fermi level and stabilization of the Pt/STO interfaces must be therefore realized by the electronic reorganization. The data in Table V confirm this as all values of $\Delta\Phi_{B,p}^{(2)}$ are large and positive and cause the Fermi level to shift inside the STO band gap for a relaxed interface. The potential shift $\Delta V^{(2)}$ arises from the rearrangement of the electron density and the formation of the interfacial dipole (strictly speaking the quantity is "dipole moment density" but we omit the full name for brevity). It should be borne in mind that our derivation of the interfacial dipole is again just one of many possible definitions of this ambiguous quantity. In fact, one has to consider always the reference with respect to which the interface dipole is determined and take it there-

TABLE V. Contributions to the SBH for the Pt/STO systems that enter Eqs. (3)–(6) (all values are in eV).

	Stage 0	Stage 1			Stage 2		
	$\Phi_{B,p}^{(0)}$	$\Delta I_S^{(1)}$	$\Delta\phi_M^{(1)}$	$\Delta\Phi_{B,p}^{(1)}$	$\Delta V^{(2)}$	$\Delta\phi_M^{(2)}$	$\Delta\Phi_{B,p}^{(2)}$
SrO term							
7 Pt	−2.00	0.36	0.00	0.36	3.38	0.00	3.38
3 Pt	−1.96	0.36	0.00	0.36	3.26	0.04	3.22
1 Pt	−2.64	0.11	−0.14	0.25	3.62	−0.51	4.13
TiO_2 term							
7 Pt	0.34	−1.14	0.00	−1.14	2.57	0.00	2.57
3 Pt	0.38	−1.13	−0.04	−1.09	2.62	0.12	2.50
1 Pt	−0.30	−1.29	0.00	−1.29	2.57	−0.77	3.34

fore as a relative rather than absolute measure.[107] The drop of the potential obtained by subtracting the planar averages of the electrostatic potential from interface and surface slabs is shown in Fig. 9. We see that for the three- and seven-layer Pt slabs the potential profiles are almost identical and the drop $\Delta V^{(2)}$ does not depend on the thickness of the metal layer but differs by almost 1 eV between the two terminations. For the monolayer coverage the potential profiles contain a small hump located at the position of the Pt layer. This feature arises due to the close proximity of interface and surface and leads to rather large deviations of the effective WF from the bulk WF (see $\Delta\phi_M^{(2)}$ in Table V).

The change in the electrostatic potential is directly related to the change in the charge (here electron) density via Poisson's equation:

$$\Delta V^{(2)} = 4\pi e^2 p_{\text{int}}, \tag{7}$$

where we define

$$p_{\text{int}} = \int z\Delta\bar{\rho}\, dz \tag{8}$$

as the interfacial dipole associated with the electronic rearrangement, i.e., in chemical language the formation of bonds between the metal and STO. This definition of the interfacial dipole has therefore a very transparent physical meaning and naturally excludes the arbitrary shifts of the average bulk electrostatic potentials.

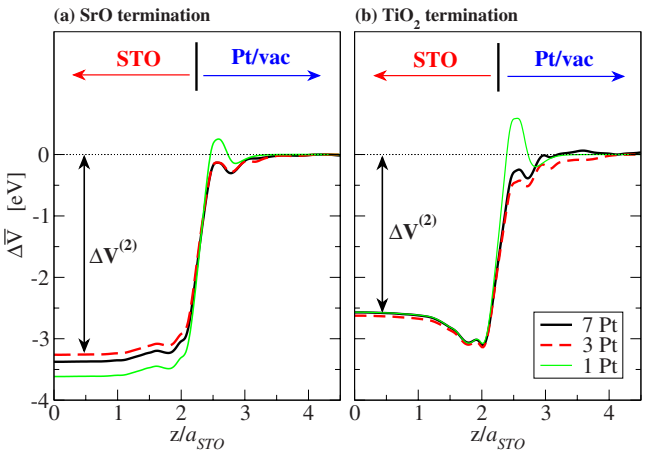

FIG. 9. (Color online) Change in the electrostatic potential due to redistribution of the electronic density during step 2 at (a) SrO-terminated and (b) TiO_2-terminated Pt/STO interfaces.

The differences of the planar averaged electron densities, which were obtained in the same way as the differences of the planar averaged electrostatic potential, are shown for the six Pt/STO interfaces in Fig. 10. It is obvious from these graphs that all charge profiles have similar characteristic features. First, the charge transfer is limited to a close vicinity of the interface and is mainly located between the interfacial planes. This strong confinement is the reason why the SBH depends only slightly on the thickness of the Pt layer. In addition, the rapid decay causes the three-layer Pt/STO system to have the same work function as the bulk platinum since the presence of the interface does not influence the surface dipole at the metal surface. Second, the electrons are transferred always from STO to Pt creating a dipole moment pointing toward STO. The same direction of charge transfer was observed by Rao *et al.*[42] for the Pt/BTO interface.

By integrating the planar averaged charge density we can obtain a cumulative charge profile across the interface and from its supremum estimate the magnitude of the charge transferred per unit area of the interface and the interface position.[105] The position of the supremum corresponds to the point where the planar charge density intercepts the x axis between the TM and STO interfacial planes (the point is marked in Fig. 10 by arrows). However, since the partition of charge is not unique the quantities can be taken only as indicative.

In summary, the step-by-step analysis that follows naturally the formation of interface is able to provide a wealth of information on the quantities that determine the SBH. The resulting value of the SBH calculated from Eq. (3) agrees well with the values determined directly (see Table IV). In the following we apply the analysis to a number of TM/STO interfaces.

C. Metal monolayers on STO

In order to investigate the dependence of the SBH on the metal electrode we carried out a series of SBH calculations

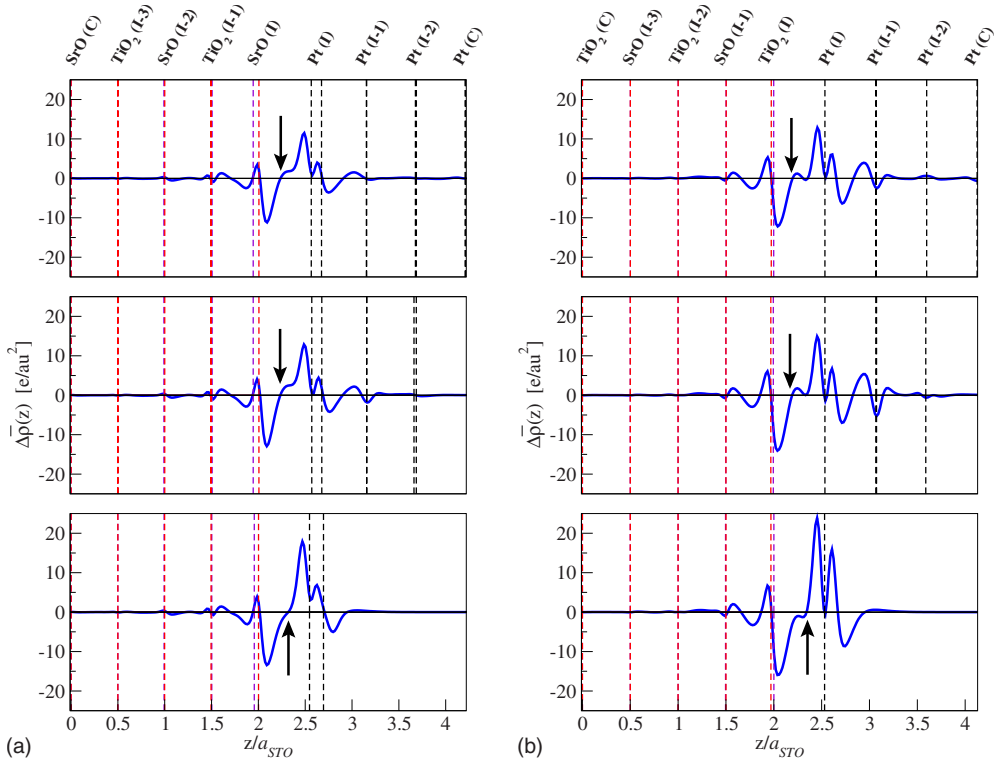

FIG. 10. (Color online) Differences of the planar averaged charge densities from the interface and slab calculations for seven-, three-, and one-layer Pt films on (a) SrO- and (b) TiO_2-terminated STO (only one half of each mirror-symmetric supercell is shown). The vertical dashed lines mark the position of atomic layers (I and C denote interface and center of the slab, respectively); the arrows indicate the interface position (see text).

for interfaces between STO and six transition metals—Cr, Mo, W, Ni, Pd, and Pt. The calculations were done for monolayer TM coverages and with supercells containing a vacuum region separating the TM/STO/TM nanocapacitors. All systems were studied in the on-top configuration with the metal deposited above the oxygen atoms. Additionally, for Mo and Pd we computed also the "hollow" configurations to explore the influence of interface geometry. The calculations were analyzed using the methodology described in the previous section.

Since metal monolayers do not have the same properties as bulk metals we computed first the WF of free-standing TM monolayers, which are necessary for determination of the ideal Schottky-Mott SBH $\Phi_{B,p}^{(0)}$ [see Eq. (5)]. The calculated monolayer WFs are listed in Table VI. These WFs are about 0.5 eV larger than those of the corresponding bulk metals (cf. Table II) indicating similar increases in the surface dipoles due to enhanced electron spillage for all six metals. When the metal monolayers are attached to STO the electron delocalization is reduced by formation of chemical bonds across the interface and the WF decreases (see the last two columns of Table VI). Interestingly, in most cases the effective WFs of the attached monolayers approach the bulk WF. Only for the hollow configuration of the SrO-terminated Mo/STO interface the effective WF remains to be about 0.6 eV larger than the bulk WF.

The key quantities associated with our step-by-step process of interface formation, i.e., the changes in the band alignment due to atomic and electronic relaxations, are summarized for all investigated monolayer interfaces in Table VII. Large variations in both terms reveal that the processes which accompany interface formation depend sensitively on the TM electrode as well as on interface termination and geometry.

The changes in the band alignment arising due to the atomic rearrangements $\Delta\Phi_{B,p}^{(1)}$ are positive for all SrO-terminated on-top interfaces but there are significant differences in the magnitude of this term for different TM. The group VI TM (Cr, Mo, and W) show much larger values than

TABLE VI. Work functions of free-standing TM monolayers $\phi_{M,\mathrm{mono}}$ and effective work functions of the TM monolayers on STO $\phi_{M,\mathrm{eff}}$ (all values are in eV).

		$\phi_{M,\mathrm{eff}}$	
	$\phi_{M,\mathrm{mono}}$	SrO	TiO_2
Cr	5.00	4.69	4.97
Mo "on-top"	5.34	4.87	5.15
Mo "hollow"		5.42	4.87
W	5.48	4.97	5.41
Ni	5.34	5.06	5.07
Pd "on-top"	6.06	5.65	5.38
Pd "hollow"		5.94	5.69
Pt	6.63	6.11	6.03

TABLE VII. Contributions to the SBH according to Eq. (3) and resulting values of the *p*-type SBH for the monolayer TM/STO interfaces; values in brackets were determined using the LM approach (all values are in eV).

	$\Phi_{B,p}^{(0)}$	$\Delta\Phi_{B,p}^{(1)}$	$\Delta\Phi_{B,p}^{(2)}$	$\Phi_{B,p}$
SrO term "on-top"				
Cr	−0.75	1.66	1.38	2.29(2.27)
Mo	−1.09	1.40	1.93	2.24(2.23)
W	−1.23	1.96	1.57	2.30(2.32)
Ni	−1.09	0.68	2.46	2.05(1.91)
Pd	−1.81	0.12	3.28	1.59(1.50)
Pt	−2.38	0.23	4.00	1.85(1.71)
TiO_2 term "on-top"				
Cr	1.52	−0.46	0.88	1.94(1.95)
Mo	1.18	−0.52	1.47	2.13(2.18)
W	1.04	−0.54	1.61	2.11(2.14)
Ni	1.18	−0.80	1.45	1.83(1.89)
Pd	0.46	−0.84	2.32	1.94(1.85)
Pt	−0.11	−1.21	3.22	1.90(1.83)
SrO term "hollow"				
Mo	−1.09	0.01	1.91	0.83(0.73)
Pd	−1.81	0.30	2.39	0.88(0.76)
TiO_2 term "hollow"				
Mo	1.18	−0.09	0.56	1.65(1.68)
Pd	0.46	−0.48	1.17	1.15(1.21)

the group X TM (Ni, Pd, and Pt) with the difference between the two groups exceeding 1 eV. Qualitatively different behavior is observed for the TiO_2-terminated on-top interfaces where $\Delta\Phi_{B,p}^{(1)}$ is always negative, again with similar values within each TM group. Apart from the large dissimilarities between the two terminations we see also a strong influence of the interface geometry. The changes due to the atomic rearrangement are much smaller for the hollow than for the on-top configurations, especially for the Mo/STO interfaces.

The electronic rearrangement term $\Delta\Phi_{B,p}^{(2)}$ is positive for all investigated interfaces but shows even larger variation in values than the $\Delta\Phi_{B,p}^{(1)}$ term. The corresponding charge transfer and interfacial dipole therefore have the same direction for all interfaces but vary significantly in magnitude for different TM and interface configurations.

Even though the variations between interfaces are large the data extracted in the analysis enable us to identify trends in the underlying mechanisms of SB formation. Establishing such trends is especially useful for the development and validation of phenomenological models that estimate the SBH using only few fundamental material parameters (see Sec. V).

In Fig. 11 we plot the crucial quantities that determine the SBH for the on-top interfaces. The triangles correspond to the characteristic properties of the metal electrode—the bulk

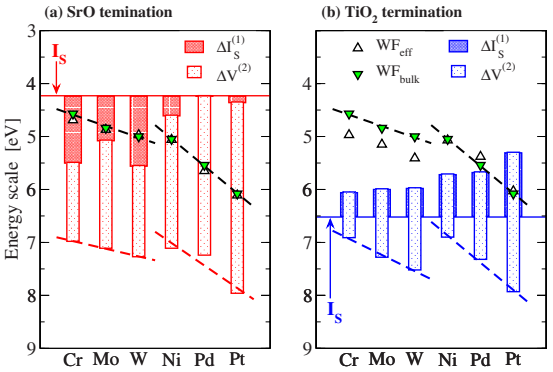

FIG. 11. (Color online) Contributions to the IP and WF for TM/STO interfaces.

and effective WFs. As was mentioned above, and as is also seen in the figure, the two WFs are in most cases almost the same and differ by a small constant shift only for the TiO_2-terminated interfaces with Cr, Mo, and W. The position of the Fermi level below the vacuum level can be taken therefore to a good approximation as independent of the metal being isolated or attached to STO. This approximation improves with thicker metal coverages (as we saw for the Pt/STO interfaces the effective WF is indistinguishable from the bulk WF already for the trilayer Pt slabs). The bulk WF thus presents indeed an independent parameter characterizing the TM.

The stacked bars in Fig. 11 represent the evolution of the second key parameter—the position of the STO valence band. The horizontal base lines on which the bars start correspond to the ionization potentials of the relaxed STO surfaces and are located 4.25 eV and 6.52 eV below the vacuum level for the SrO and TiO_2 terminations, respectively (the values are slightly different from those in Table III because seven- instead of nine-layer STO slabs were used for the monolayer-TM/STO calculations). The difference between the base line (IP) and the triangles (WF) equals to the ideal SBH $\Phi_{B,p}^{(0)}$ [see Eq. (4)]. This difference is negative for all SrO-terminated and positive for all TiO_2-terminated interfaces. The heights of the filled and empty bars then correspond to the shifts of the STO valence band due to atomic ($\Delta I_S^{(1)}$) and electronic ($\Delta V^{(2)}$) rearrangements, respectively. Figure 11 shows that even though individually the two terms vary strongly among the interfaces (especially for the SrO-terminated ones), their sum correlates very well with the metal WF for interfaces with the same termination and the same TM group. The dashed lines, which are linear interpolations of the bulk WFs and the STO valence-band maxima in the four groups of interfaces, help to see these correlations.

The relation between the total correction $\Delta\Phi_{B,p}=\Delta\Phi_{B,p}^{(1)}+\Delta\Phi_{B,p}^{(2)}$ and the bulk metal WF is plotted explicitly in Fig. 12. We can indeed see a clear linear relationship for the four interface groups but the slopes and shifts of the lines differ. Furthermore, all hollow interfaces exhibit significantly lower $\Delta\Phi_{B,p}$ values than the on-top interfaces. These results indicate that the interface dipole depends sensitively on the structure and chemical bonding at TM/STO interfaces. This fact has important implications for theoretical predictions of

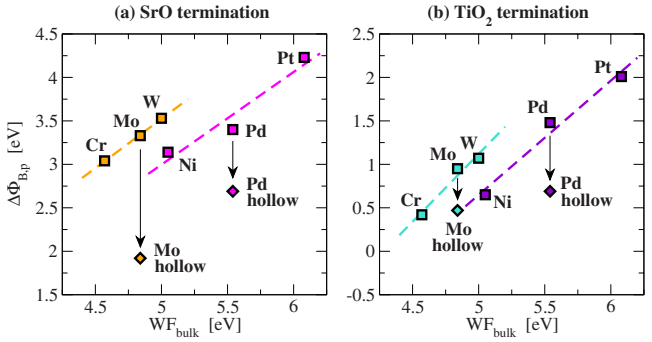

FIG. 12. (Color online) Correlation between the metal WFs and the total change in the band alignment due to the atomic and electronic rearrangements at the interface.

SBH with existing empirical theories, which we discuss in the next section.

Finally, Table VII also contains the values of SBH determined from Eq. (3) as well as by the LM approach. Similarly as for the Pt/STO interfaces both methods give consistent results of SBH for all monolayer-TM/STO interfaces.

V. EMPIRICAL THEORIES

There exist a number of phenomenological theories that try to estimate the SBH from few characteristic material parameters. These theories were originally developed for metal-semiconductor interfaces[26,27,117–122] but they have been used also for the estimation of SBH at interfaces between metals and TM oxides.[40,41,43,114,115,123] An excellent review of existing theories has been given by Tung[63] and we will therefore summarize here only the fundamental ideas on which these approaches rely.

As we already mentioned earlier the Schottky-Mott limit, which assumes no charge transfer across the interface, can be considered as an ideal, zeroth-order theory. In reality some interaction between the materials forming the interface always takes place and this interaction alters the band alignment. It has been observed experimentally that the deviation from the Schottky-Mott limit increases with increasing covalency of the semiconductor or insulator. For most covalent materials the SBH is largely independent of the metal WF and the metal Fermi level instead tends to align with some characteristic level within the insulator band gap. This phenomenon is known as Fermi level pinning (FLP). The origin and extent of the FLP present the key ingredients of most phenomenological models of SBH.

The pinning mechanisms can be essentially divided into two categories: (1) intrinsic due to the so-called metal-induced gap states (MIGS) and (2) extrinsic due to native defect or surface states. It is believed that the intrinsic pinning gives a better description of the SBH in most cases and applies also for our ideal, defect-free interfaces. The MIGS, first proposed by Heine,[124] are tails of metallic wave functions which decay exponentially into the insulator due to lack of matching insulator bulk states. Even though these gap states are induced by the metal their distribution is an intrinsic property of the insulator. The energy below which all MIGS must be filled for a charge neutral surface defines the charge neutrality level (CNL).[118] The CNL presents a key concept in the empirical theories of SBH as its role at the interface is equivalent to the metal's Fermi level. The p-type SBH is then expressed within the FLP theory as[117]

$$\Phi_{B,p} = S(I_S - \phi_M) + (1 - S)\phi_{\mathrm{CNL}}, \tag{9}$$

where S is a dimensionless Schottky pinning (or interface behavior) parameter that depends on the density and extent of the interfacial states in the insulator,[117] and ϕ_{CNL} is the energy of the charge neutrality level above the VBM of STO. The pinning factor S is characteristic for the insulator and may take on values between 0 and 1. For $S=1$ there is no charge transfer and Eq. (9) corresponds to the Schottky-Mott limit. For $S=0$ the metal Fermi level is completely pinned by the interface states at ϕ_{CNL} (Bardeen limit[125]). The n-type SBH is in this case the difference between the CNL below the vacuum level and the electron affinity of insulator. The pinning factor S can be derived from experimental dependence of the SBH on the WF ($-S=\partial\Phi_{B,p}/\partial\phi_M$) or estimated using an empirical formula:[122]

$$S = \frac{1}{1 + 0.1(\epsilon_\infty - 1)^2} \tag{10}$$

with ϵ_∞ being the electronic dielectric constant. Reported values of S for STO range between 0.1 and 0.6[18,94,119,126] with the empirical estimate of 0.28.[114] This range of values corresponds to a moderate FLP. A consistent procedure to determine the CNL is not available and several methods have been proposed.[63] Robertson and Chen[114,115] and Demkov *et al.*[127] calculated the CNL for STO from the branch point of the complex band structure[128] to be 2.6 and 0.7–1.3 eV above the VBM, respectively.

Even though the MIGS model has been applied successfully to a variety of metal-semiconductor interfaces it incorrectly assumes that chemical bonds formed at the interface have no impact on the interface dipole since the distribution of the gap states, which pin the Fermi level, is an innate property of the semiconductor. However, both first-principles and experimental data for epitaxial metal-semiconductor interfaces have indicated that the SBH depends on the interfacial atomic structure and details of chemical bonding (for a summary see Refs. 8 and 63).

Recently, Tung[94,129] proposed a novel approach based on the polarization of interfacial bonds. His bond polarization theory is able to account for the FLP phenomenon and at the same time removes the internal inconsistencies of the classical MIGS models. The basic principle of Tung's formulation is identical to other SB theories, namely, that the frozen charge distribution of the Schottky-Mott limit needs to relax for minimizing the interfacial energy. The charge rearrangement is the source of an interface dipole D_{int}, which causes the deviation of the SBH from the ideal Schottky-Mott limit as

$$\Phi_{B,p} = I_S - \phi_M - eD_{\mathrm{int}}. \tag{11}$$

The bond polarization theory assumes that the major charge rearrangement originates from the formation of polarized chemical bonds across the interface. The interface dipole

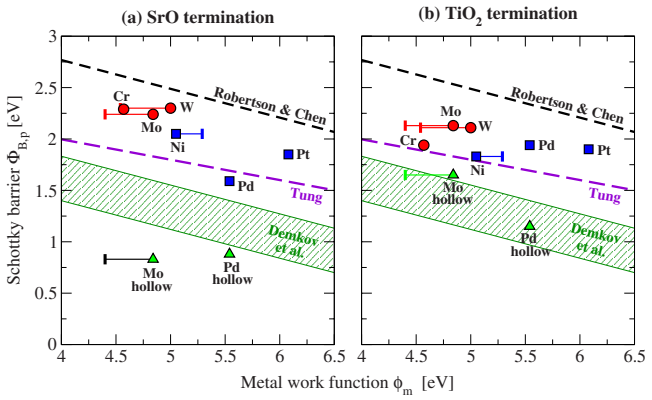

FIG. 13. (Color online) Comparison of SBH from DFT calculations (points) with empirical estimates of Robertson and Chen (Refs. 114 and 115), Demkov *et al.* (Refs. 40 and 126), and Tung (Ref. 94). The error bars at the DFT values mark the range of calculated WFs for different lateral lattice parameters of the TM (see Table III).

then can be determined by considering the interface region as a giant molecule and using a simple picture of charge transfer:

$$D_{\text{int}} = \frac{eq_{\text{int}}d_{\text{int}}N_B}{\epsilon_{\text{int}}}, \tag{12}$$

where q_{int} is the charge transferred between atoms participating in interfacial bonds, d_{int} is the interface separation, N_B is the bond density, and ϵ_{int} is the dielectric constant of the interface region. By expressing the transferred charge in terms of bulk crystal properties Tung obtained a dependence of the SBH on the metal WF,

$$\Phi_{B,p} = S(I_S - \phi_M) + (1 - S)\frac{E_g}{2}, \tag{13}$$

which is similar to Eq. (9) with half of the band gap $E_g/2$ replacing the CNL. This model thus leads to a weak dependence of the SBH on the work function and a natural tendency for the SBH to converge toward the middle of the band gap. The interface parameter S is however different from that predicted by the MIGS models.

Our first-principles calculations and the analysis we presented in the previous section enable us to probe both the numerical predictions and the underlying assumptions of these phenomenological models. The comparison of the first-principles and empirical SBH plotted as a function of the metal WF is shown in Fig. 13. Even though both MIGS models exhibit the same decrease in the p-type SBH with increasing metal WF (due to the same interface pinning parameter S) the range of predicted SBH differs by more than 1 eV. An origin of this large difference can be traced to the uncertainty in determination of the CNL position. While Robertson and Chen[114,115] obtained the CNL level close to the conduction-band edge of STO, Zhang *et al.*[126] found it to be only about 0.7 eV above the valence-band edge (with an uncertain LDA correction). The first-principles SBH for the on-top TM/STO interfaces fall between these two extremes. Within the phenomenological picture of FLP these interfaces would therefore correspond to a strong pinning limit with the CNL located close to the middle of the band gap. This view however breaks down when we consider the hollow-type interfaces. Their first-principles SBH, especially for the SrO-terminated interfaces, are much lower than the SBH of the on-top-type interfaces pointing to the inability of the simple MIGS models to describe correctly the mechanisms responsible for the SB formation.

The first-principles results appear more consistent with the basic assumptions of the bond polarization theory. The linear dependence of the SBH on the WF shown in Fig. 13 was obtained for an empirical value of the interface behavior parameter $S=0.2$. This parameter is however not unique in the bond polarization theory and depends on the chemical bonds established at the interface [see Eq. (12)]. The relatively good agreement visible in Fig. 13 for the on-top interfaces is rather fortuitous and related to the fact that the atomic structure and chemical bonding in this group of interfaces is quite similar. In fact, we can determine the appropriate values of S from the analysis described in the previous section. The slopes of lines obtained by linear interpolations of $\Delta\Phi_{B,p}$ (see Fig. 12) correspond directly to $1-S$. The bond polarization theory is also able to provide a plausible explanation of the lower SBH values for the hollow interfaces. These interfaces contain a lower density of interfacial bonds between the TM and oxygen, and consequently, the interface dipole is smaller. The reduced bond density leads also to a weaker FLP.

An interesting result of our analysis is the importance of atomic rearrangements. The bond polarization theory considers the charge rearrangement, which arises from the formation of interfacial bonds, as the only contribution to the interface dipole. Our analysis reveals that the dipole associated with atomic rearrangements may be of the same order of magnitude and is therefore not negligible. A deeper analysis will be the subject of a forthcoming paper.

VI. CONCLUSIONS

We have evaluated the Schottky barrier heights for a number of TM/STO interfaces by first-principles DFT calculations. Our results show that the interface band alignment depends sensitively on the interface structure and chemistry. The step-by-step analysis of the interface formation enables us to separate the contributions to the SBH originating from the atomic and electronic rearrangements at the interfaces. A comparison of the calculated SBH with predictions of the existing phenomenological theories reveals the inability of simple MIGS models to describe correctly the mechanisms responsible for the SB formation.

ACKNOWLEDGMENTS

Financial support for this work was provided by the German Research Foundation (DFG) through Project No. El 155/17-2 in the priority program 1157 "Integrated electroceramic functional structures," and by the European Commission through Contract No. NMP3-CT-2005-013862 (INCEMS). We would like to thank Tony Paxton for valuable comments.

*matous.mrovec@iwm.fraunhofer.de

[1] N. Setter and R. Waser, Acta Mater. **48**, 151 (2000).
[2] T. M. Shaw, S. Trolier-McKinstry, and P. C. McIntyre, Annu. Rev. Mater. Sci. **30**, 263 (2000).
[3] *Nanoelectronics and Information Technology: Advanced Electronic Materials and Novel Devices*, edited by R. Waser (Wiley-VCH, Weinheim, 2003).
[4] G. D. Wilk, R. M. Wallace, and J. M. Anthony, J. Appl. Phys. **89**, 5243 (2001).
[5] R. A. McKee, F. J. Walker, and M. F. Chisholm, Phys. Rev. Lett. **81**, 3014 (1998).
[6] F. Pan, D. Olaya, J. C. Price, and C. T. Rogers, Appl. Phys. Lett. **84**, 1573 (2004).
[7] K. Ueno, I. Inoue, H. Akoh, M. Kawasaki, Y. Tokura, and H. Takagi, Appl. Phys. Lett. **83**, 1755 (2003).
[8] Q. Fu and T. Wagner, Surf. Sci. Rep. **62**, 431 (2007).
[9] D. Deak, Mater. Sci. Technol. **23**, 127 (2007).
[10] G. W. Dietz and R. Waser, Integr. Ferroelectr. **8**, 317 (1995).
[11] K. Abe and S. Komatsu, Jpn. J. Appl. Phys. **32**, 4186 (1993).
[12] S. Yamamichi, T. Sakuma, K. Takemura, and Y. Miysaka, Jpn. J. Appl. Phys. **30**, 2193 (1991).
[13] K. Abe and S. Komatsu, Jpn. J. Appl. Phys. **31**, 2985 (1992).
[14] G. W. Dietz, M. Schumacher, R. Waser, S. K. Streiffer, C. Basceri, and A. I. Kingon, J. Appl. Phys. **82**, 2359 (1997).
[15] G. W. Dietz and R. Waser, Thin Solid Films **299**, 53 (1997).
[16] M. Copel, P. R. Duncombe, D. A. Neumayer, T. M. Shaw, and R. M. Tromp, Appl. Phys. Lett. **70**, 3227 (1997).
[17] C. S. Hwang, B. T. Lee, C. S. Kang, J. W. Kim, K. H. Lee, H.-J. Cho, H. Horii, W. D. Kim, S. I. Lee, Y. B. Roh, and M. Y. Lee, J. Appl. Phys. **83**, 3703 (1998).
[18] J. F. Scott, Jpn. J. Appl. Phys. **38**, 2272 (1999).
[19] T. Shimizu and H. Okushi, J. Appl. Phys. **85**, 7244 (1999).
[20] A. Yoshida, H. Tamura, K. Gotoh, H. Takauchi, and S. Hasuo, J. Appl. Phys. **70**, 4976 (1991).
[21] S. Gopalan, V. Balu, J. Lee, J. Hee-Han, and J. Lee, Appl. Phys. Lett. **77**, 1526 (2000).
[22] C. Park, Y. Seo, J. Jung, and D.-W. Kim, J. Appl. Phys. **103**, 054106 (2008).
[23] R. Schafranek and A. Klein, Solid State Ion. **177**, 1659 (2006).
[24] R. Schafranek, S. Payan, M. Maglione, and A. Klein, Phys. Rev. B **77**, 195310 (2008).
[25] C. S. Hwang, J. Appl. Phys. **92**, 432 (2002).
[26] S. B. Zhang, M. L. Cohen, and S. G. Louie, Phys. Rev. B **32**, 3955 (1985).
[27] S. G. Louie and M. L. Cohen, Phys. Rev. Lett. **35**, 866 (1975).
[28] S. G. Louie, J. R. Chelikowsky, and M. L. Cohen, Phys. Rev. B **15**, 2154 (1977).
[29] J. Ihm, S. G. Louie, and M. L. Cohen, Phys. Rev. Lett. **40**, 1208 (1978).
[30] G. P. Das, P. Blöchl, O. K. Andersen, N. E. Christensen, and O. Gunnarsson, Phys. Rev. Lett. **63**, 1168 (1989).
[31] M. van Schilfgaarde and N. Newman, Phys. Rev. Lett. **65**, 2728 (1990).
[32] S. Picozzi, A. Continenza, G. Satta, S. Massidda, and A. J. Freeman, Phys. Rev. B **61**, 16736 (2000).
[33] C. Berthod, N. Binggeli, and A. Baldereschi, Europhys. Lett. **36**, 67 (1996).
[34] S. Picozzi, G. Profeta, A. Continenza, S. Massidda, and A. J. Freeman, Phys. Rev. B **65**, 165316 (2002).
[35] H. Fujitani and S. Asano, Phys. Rev. B **42**, 1696 (1990).
[36] M. Nunez and M. Buongiorno Nardelli, Phys. Rev. B **73**, 235422 (2006).
[37] J. Goniakowski and C. Noguera, Interface Sci. **12**, 93 (2004).
[38] L. Giordano, M. Baistrocchi, and G. Pacchioni, Phys. Rev. B **72**, 115403 (2005).
[39] L. Giordano, F. Cinquini, and G. Pacchioni, Phys. Rev. B **73**, 045414 (2006).
[40] A. A. Demkov, Phys. Rev. B **74**, 085310 (2006).
[41] K. Y. Tse and J. Robertson, Phys. Rev. Lett. **99**, 086805 (2007).
[42] F. Y. Rao, M. Y. Kim, A. J. Freeman, S. P. Tang, and M. Anthony, Phys. Rev. B **55**, 13953 (1997).
[43] S. Clark and J. Robertson, Appl. Phys. Lett. **90**, 132903 (2007).
[44] M. Stengel and N. Spaldin, Nature (London) **443**, 679 (2006).
[45] Y. F. Dong, Y. Y. Mi, Y. P. Feng, A. C. H. Huan, and S. J. Wang, Appl. Phys. Lett. **89**, 122115 (2006).
[46] C. Elsässer, N. Takeuchi, K. M. Ho, C. T. Chan, P. Braun, and M. Fähnle, J. Phys.: Condens. Matter **2**, 4371 (1990).
[47] K. M. Ho, C. Elsässer, C. T. Chan, and M. Fähnle, J. Phys.: Condens. Matter **4**, 5189 (1992).
[48] B. Meyer, C. Elsässer, F. Lechermann, and M. Fähnle, Fortran90 Program for Mixed-Basis Pseudopotential Calculations for Crystals, Max-Planck-Institut für Metallforschung Stuttgart.
[49] D. M. Ceperley and B. J. Alder, Phys. Rev. Lett. **45**, 566 (1980).
[50] J. P. Perdew and A. Zunger, Phys. Rev. B **23**, 5048 (1981).
[51] S. G. Louie, K. M. Ho, and M. L. Cohen, Phys. Rev. B **19**, 1774 (1979).
[52] C. L. Fu and K. M. Ho, Phys. Rev. B **28**, 5480 (1983).
[53] D. Vanderbilt, Phys. Rev. B **32**, 8412 (1985).
[54] T. Ochs and C. Elsässer, Z. Metallk. **93**, 406 (2002).
[55] S. Hutt, S. Köstlmeier, and C. Elsässer, J. Phys.: Condens. Matter **13**, 3949 (2001).
[56] C. Elsässer, M. Fähnle, C. T. Chan, and K. M. Ho, Phys. Rev. B **49**, 13975 (1994).
[57] A. Polli, T. Wagner, T. Gemming, and M. Rühle, Surf. Sci. **448**, 279 (2000).
[58] T. Ochs, S. Köstlmeier, and C. Elsässer, Integr. Ferroelectr. **32**, 267 (2001).
[59] T. Classen and C. Elsässer (unpublished).
[60] A. Asthagiri and D. S. Sholl, J. Chem. Phys. **116**, 9914 (2002).
[61] T. Wagner, G. Richter, and M. Rühle, J. Appl. Phys. **89**, 2606 (2001).
[62] K. van Benthem, C. Elsässer, and M. Rühle, Phys. Rev. B **72**, 125435 (2005).
[63] R. T. Tung, Mater. Sci. Eng., R. **35**, 1 (2001).
[64] M. Methfessel, D. Hennig, and M. Scheffler, Phys. Rev. B **46**, 4816 (1992).
[65] E. Wimmer, A. J. Freeman, J. R. Hiskes, and A. M. Karo, Phys. Rev. B **28**, 3074 (1983).
[66] H. L. Skriver and N. M. Rosengaard, Phys. Rev. B **46**, 7157 (1992).
[67] M. Weinert and A. J. Freeman, Phys. Rev. B **28**, 6262 (1983).
[68] C. Fall, N. Binggeli, and A. Baldereschi, J. Phys.: Condens. Matter **11**, 2689 (1999).
[69] T. C. Leung, C. L. Kao, W. S. Su, Y. J. Feng, and C. T. Chan, Phys. Rev. B **68**, 195408 (2003).
[70] P. J. Feibelman and D. R. Hamann, Phys. Rev. B **29**, 6463 (1984).
[71] R. J. Wilson and A. P. Mills, Surf. Sci. **128**, 70 (1983).
[72] H. B. Michaelson, J. Appl. Phys. **48**, 4729 (1977).
[73] H. Kawano, Prog. Surf. Sci. **83**, 1 (2008).

[74] T. Ohwaki, D. Wortmann, H. Ishida, S. Blügel, and K. Terakura, Phys. Rev. B **73**, 235424 (2006).
[75] K. Wandelt, *Thin Metal Films and Gas Chemisorption* (Elsevier, Amsterdam, 1987), p. 307.
[76] R. Smoluchowski, Phys. Rev. **60**, 661 (1941).
[77] K. Johnston, M. R. Castell, A. T. Paxton, and M. W. Finnis, Phys. Rev. B **70**, 085415 (2004).
[78] E. Heifets, S. Piskunov, E. A. Kotomin, Y. F. Zhukovskii, and D. E. Ellis, Phys. Rev. B **75**, 115417 (2007).
[79] R. Herger, P. R. Willmott, O. Bunk, C. M. Schleputz, B. D. Patterson, B. Delley, V. L. Shneerson, P. F. Lyman, and D. K. Saldin, Phys. Rev. B **76**, 195435 (2007).
[80] D. Bonnell and J. Garra, Rep. Prog. Phys. **71**, 044501 (2008).
[81] O. Warschkow, M. Asta, N. Erdman, K. R. Poeppelmeier, D. E. Ellis, and L. D. Marks, Surf. Sci. **573**, 446 (2004).
[82] T. Kubo and H. Nozoye, Surf. Sci. **542**, 177 (2003).
[83] J. Goniakowski, F. Finocchi, and C. Noguera, Rep. Prog. Phys. **71**, 016501 (2008).
[84] E. Heifets, R. I. Eglitis, E. A. Kotomin, J. Maier, and G. Borstel, Phys. Rev. B **64**, 235417 (2001).
[85] E. Heifets, R. Eglitis, E. Kotomin, J. Maier, and G. Borstel, Surf. Sci. **513**, 211 (2002).
[86] J. Padilla and D. Vanderbilt, Surf. Sci. **418**, 64 (1998).
[87] Z.-Q. Li, J.-L. Zhu, C. Q. Wu, Z. Tang, and Y. Kawazoe, Phys. Rev. B **58**, 8075 (1998).
[88] R. I. Eglitis and D. Vanderbilt, Phys. Rev. B **77**, 195408 (2008).
[89] C. Cheng, K. Kunc, and M. H. Lee, Phys. Rev. B **62**, 10409 (2000).
[90] S. Massidda, B. I. Min, and A. J. Freeman, Phys. Rev. B **35**, 9871 (1987).
[91] A. Balderschi, S. Baroni, and R. Resta, Phys. Rev. Lett. **61**, 734 (1988).
[92] L. Colombo, R. Resta, and S. Baroni, Phys. Rev. B **44**, 5572 (1991).
[93] J. M. Albina, M. Mrovec, B. Meyer, and C. Elsässer, Phys. Rev. B **76**, 165103 (2007).
[94] R. T. Tung, Phys. Rev. B **64**, 205310 (2001).
[95] C. Sgiarovello, N. Binggeli, and A. Baldereschi, Phys. Rev. B **64**, 195305 (2001).
[96] J. Van Vechten, J. Vac. Sci. Technol. B **3**, 1240 (1985).
[97] W. Egelhoff, Surf. Sci. Rep. **6**, 253 (1987).
[98] K. van Benthem, C. Elsässer, and R. H. French, J. Appl. Phys. **90**, 6156 (2001).
[99] G. Cappellini, S. Bouette-Russo, B. Amadon, C. Noguera, and F. Finocchi, J. Phys.: Condens. Matter **12**, 3671 (2000).
[100] C. Sgiarovello, N. Binggeli, and A. Baldereschi, Phys. Rev. B **69**, 035320 (2004).
[101] V. E. Henrich, G. Dresselhaus, and H. J. Zeiger, Phys. Rev. B **17**, 4908 (1978).
[102] Y.-W. Chung and W. B. Weissbard, Phys. Rev. B **20**, 3456 (1979).
[103] S. Piskunov, E. Kotomin, E. Heifets, J. Maier, R. Eglitis, and G. Borstel, Surf. Sci. **575**, 75 (2005).
[104] B. Baumeier, P. Krüger, and J. Pollmann, Phys. Rev. B **76**, 205404 (2007).
[105] J. Junquera, M. Cohen, and K. Rabe, J. Phys.: Condens. Matter **19**, 213203 (2007).
[106] M. Peressi, N. Binggeli, and A. Baldereschi, J. Phys. D **31**, 1273 (1998).
[107] A. Franciosi and C. G. Van de Walle, Surf. Sci. Rep. **25**, 1 (1996).
[108] A. Baldereschi, M. Peressi, S. Baroni, and R. Resta, *Proceedings of the International School of Physics "Enrico Fermi," Course CXVII, Varenna, 1991*, edited by L. Migli and A. Stella (Academic, New York, 1993), p. 59.
[109] P. J. Møller, S. A. Komolov, E. F. Lazneva, and A. S. Komolov, Appl. Surf. Sci. **175-176**, 663 (2001).
[110] W. Maus-Friedrichs, M. Frerichs, A. Gunhold, S. Krischok, V. Kempter, and G. Bihlmayer, Surf. Sci. **515**, 499 (2002).
[111] Of course, in real calculations the two steps are performed in a reversed order—the interface is first relaxed and after that the two materials are separated.
[112] A. Asthagiri, C. Niederberger, A. J. Francis, L. M. Porter, P. A. Salvador, and D. S. Sholl, Surf. Sci. **537**, 134 (2003).
[113] A. Asthagiri and D. S. Sholl, J. Mol. Catal. Chem. **216**, 233 (2004).
[114] J. Robertson and C. W. Chen, Appl. Phys. Lett. **74**, 1168 (1999).
[115] J. Robertson, J. Vac. Sci. Technol. B **18**, 1785 (2000).
[116] Y. F. Dong, S. J. Wang, Y. P. Feng, and A. C. H. Huan, Phys. Rev. B **73**, 045302 (2006).
[117] A. Cowley and S. Sze, J. Appl. Phys. **36**, 3212 (1965).
[118] C. Tejedor, F. Flores, and E. Louis, J. Phys. C **10**, 2163 (1977).
[119] M. Schlüter, Phys. Rev. B **17**, 5044 (1978).
[120] J. Tersoff, Phys. Rev. Lett. **52**, 465 (1984).
[121] F. Flores and C. Tejedor, J. Phys. C **20**, 145 (1987).
[122] W. Mönch, Phys. Rev. Lett. **58**, 1260 (1987).
[123] M. Dawber and J. F. Scott, Jpn. J. Appl. Phys. **41**, 6848 (2002).
[124] V. Heine, Phys. Rev. **138**, A1689 (1965).
[125] J. Bardeen, Phys. Rev. **71**, 717 (1947).
[126] X. Zhang, A. A. Demkov, H. Li, X. Hu, Y. Wei, and J. Kulik, Phys. Rev. B **68**, 125323 (2003).
[127] A. A. Demkov, L. R. C. Fonseca, E. Verret, J. Tomfohr, and O. F. Sankey, Phys. Rev. B **71**, 195306 (2005).
[128] J. Tersoff, Phys. Rev. B **30**, 4874 (1984).
[129] R. T. Tung, Phys. Rev. Lett. **84**, 6078 (2000).